Available online at www.sciencedirect.com
ScienceDirect
European Journal of Mechanics B/Fluids 26 (2007) 220–235

On axisymmetric intrusive gravity currents in a stratified ambient – shallow-water theory and numerical results

Marius Ungarish *, Tamar Zemach

Department of Computer Science, Technion, Haifa 32000, Israel

Received 17 July 2005; received in revised form 26 April 2006; accepted 9 June 2006

Available online 8 August 2006

Abstract

The intrusion of a fixed volume of fluid, which is released from rest and then propagates horizontally-radially at the neutral buoyancy level in a stratified ambient fluid, in a cylindrical geometry with a vertical axis (either fully axisymmetric or a wedge), is investigated. It is assumed that the density change of the ambient fluid is linear with height. A closed one-layer shallow-water Boussinesq inviscid formulation is presented. In general, the solution of the resulting hyperbolic system is obtained by a finite-difference scheme. However, for the large-time developed motion an analytical similarity solutions is derived. The self-similar result indicates radial expansion with $t^{1/3}$ but the shape is peculiar: the intruding fluid propagates like a ring with a fixed ratio of inner to outer radii; the inner domain (between the axis and the inner radius of the ring) contains clear ambient fluid. It is verified that the initial-value lock-release finite-difference solution indeed approaches the similarity predictions after an initial spread of the outer radius to about 2.5 times the initial radius. The shallow-water results are corroborated by numerical solutions of the full axisymmetric Navier–Stokes formulation. It is concluded that the shallow-water model is a versatile and accurate predictive tool, and that the peculiar ring-shape prediction reproduces an interesting physical property of the axisymmetric intrusion. The interaction between the internal gravity waves and the head is less significant than in the two-dimensional geometry. However, a practical limitation on the applicability of the inviscid model is imposed by the prediction that the ratio of viscous to inertia forces increases like r_N^7 (where r_N is the radius of propagation, scaled with the initial value).

Keywords: Gravity current; Intrusion; Stratified; Self-similar; Shallow water

1. Introduction

We consider the mainly horizontal-radial motion which develops when a given volume of fluid of constant density is released into a vertically stratified ambient at the level of neutral buoyancy, in a cylindrical geometry. The propagation starts from rest in a region of radial dimension r_0 about the axis, and the velocity has no lateral (azimuthal) component. The typical configuration is sketched in Fig. 1. We assume that the density of the ambient fluid varies linearly over the full depth of the container, and that the Reynolds number of the flow (defined below) is large. The intrusion

* Corresponding author.
E-mail address: unga@cs.technion.ac.il (M. Ungarish).

0997-7546/$ – see front matter
doi:10.1016/j.euromechflu.2006.06.003

under consideration is a special case of flows called gravity currents, and is a well-known phenomenon in natural and industrial systems (see Simpson [1]).

The previous investigations of intrusions released from behind a lock into a stratified ambient were concerned mainly with the two-dimensional flow in Cartesian (rectangular) configurations (e.g., Wu [2], Kao [3], Manins [4], Amen and Maxworthy [5], Faust and Plate [6], deRooij [7]). The related studies in the axisymmetric configuration (see Ivey and Blake [8] and Lemckert and Imberger [9] where other relevant references are given) were focused on source-sink flow-fields, which are very different from the lock-release case.

Even for the two-dimensional case the "state of the art" of theoretical interpretation and prediction was unsatisfactory, as stated by Faust and Plate [6]: "intrusions into a linearly stratified environment behave very differently from theoretical calculations". Some encouraging progress was attained by Ungarish [10], by means of a one-layer shallow-water model, supported by Navier–Stokes simulations. This approach clarifies and quite accurately reproduces many of the observed features of the propagation (e.g, motion with constant velocity, the influence of the shape of the lock, sub-criticality of the speed as compared with the fastest internal gravity wave, etc.). Here we present an extension of this analysis to the axisymmetric geometry. Besides the academic interest, the insights into this problem are also expected to be relevant to practical circumstances such as propagation of pollutants. Indeed, in many environmental intrusions the axisymmetric geometry (either a full cylinder or a part of it as a wedge) seems more relevant than the rectangular one.

The extension from the rectangular to the axisymmetric geometry is non-trivial and produces some unexpected results. The intruding fluid diverges as a result of the radial propagation and hence the balances along the characteristics of the SW model contain time-dependent source terms. The predicted velocity field and the shape of the interface gain some complexities with have no counterpart in the Cartesian case. Nevertheless, we show that a self-similar behavior emerges. The NS simulations confirm these features and the accuracy of the predicted radius of propagation as a function of time.

The structure of the paper is as follows. In Section 2 the shallow-water equations of motion and the appropriate boundary conditions are presented. The self-similar analytical solution (for large times) of this system is developed and discussed. In Section 3 some detailed finite-difference results of the SW initial-value problem (release from rest) are presented and compared with (a) the similarity analytical results for a deep intrusion, and (b) with the NS simulation for a non-deep intrusion. Concluding remarks are given in Section 4. Some contrasting results in the corresponding rectangular geometry are briefly displayed in Appendix A.

2. Formulation and SW approximations

The configuration is sketched in Fig. 1. We use a $\{r, \theta, z\}$ cylindrical coordinate system with corresponding $\{u, v, w\}$ velocity components. The gravity acts in the $-z$ direction. We assume that the geometry is fully axisymmetric about the axis z, or a wedge with smooth vertical sidewalls rz planes (in the latter case, the gap at $r = r_0$ is large as

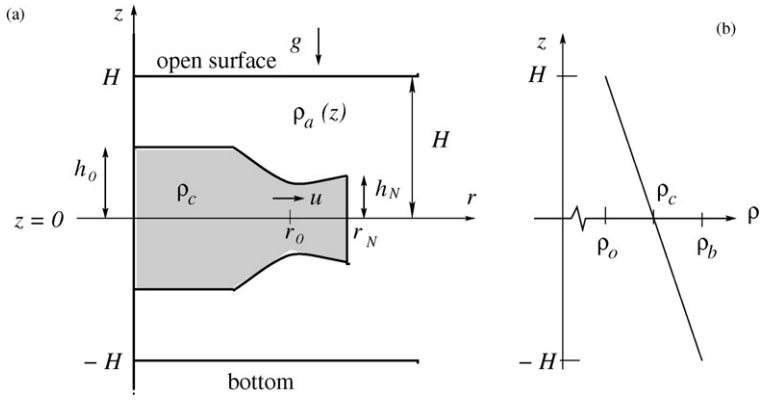

Fig. 1. Schematic description of the system (a) the geometry; (b) density profile in the ambient. In dimensionless form, the horizontal lengths are scaled with r_0 and the vertical lengths with h_0. The subscripts denote: N – nose (or front); a – ambient; b – bottom; c – current (intrusion); o – open surface.

compared with the thickness of the intrusion, h_0). The inviscid flow does not depend on the coordinate θ, and $v \equiv 0$. We refer to this configuration as axisymmetric.

The initial flow-field configuration is symmetric with respect to the horizontal plane $z = 0$. The ambient fluid is in the domain $-H \leqslant z \leqslant H$, and is stably stratified; for simplicity, the density increase occurs linearly from ρ_o to ρ_b. The initial position of the intrusive fluid is in a lock $0 \leqslant r \leqslant r_0$. Unless stated otherwise, the lock is a cylinder $-h_0 \leqslant z \leqslant h_0$. The density of the intruding current is equal to that of the ambient at the symmetry plane $z = 0$. In this respect, the fluid of the intrusion can be regarded as the result of mixing the ambient in the lock, and is also referred to as the "mixed fluid". This can be expressed as

$$\rho_c = \rho_a(z = 0) = \frac{1}{2}(\rho_o + \rho_b), \tag{2.1}$$

where the subscript a denotes the ambient and c, b, o refer to values of the current (or intrusion, or mixed), bottom and open surface. It is convenient to use ρ_o as the reference density.

We introduce the reduced gravity,

$$g' = \epsilon g, \tag{2.2}$$

where g is the gravitational acceleration and

$$\epsilon = \frac{\rho_c - \rho_o}{\rho_o}, \tag{2.3}$$

is the dimensionless density difference.

The density in the intruding current and in the ambient can be expressed as

$$\rho_c = \rho_o(1 + \epsilon), \qquad \rho_a = \rho_o\left[1 + \epsilon\left(1 - \frac{z}{H}\right)\right]. \tag{2.4}$$

The buoyancy frequency is constant and given by

$$\mathcal{N} = \left(\frac{g'}{H}\right)^{1/2}, \tag{2.5}$$

where H is the dimensional thickness of the ambient fluid above (and below) the neutral buoyancy level midplane, $z = 0$. The speed of the fastest internal wave is $\mathcal{N}H/\pi$ (we use here the linear mode 2 wave in a stratified layer symmetric about $z = 0$, see Amen and Maxworthy [5] and Baines [11]).

The following shallow-water approximations are concerned with the inviscid ($Re \gg 1$; the Reynolds number is defined below), and Boussinesq ($\epsilon \ll 1$) limits. In this case the initial symmetry about $z = 0$ is expected to prevail also during the time-dependent propagation. It is therefore sufficient to consider the flow in the domain $z \geqslant 0$. The shape of the density interface and the velocity field in the domain $z \leqslant 0$ are expected to be mirror images.

For the rectangular two-dimensional counterpart problem Ungarish [10] developed a one-layer shallow-water approximation. This is the simplest shallow-water model, which ignores the motion in the ambient fluid. However, it was shown that it captured well many of the important features of the flow of the dense fluid. This theoretical approach is adopted here, subject to the changes imposed by the different geometry.

In the ambient fluid domain we assume that $u = v = w = 0$ and hence the fluid is in purely hydrostatic balance and maintains the initial density $\rho_a(z)$. The motion is assumed to take place in the intruding layer of fluid only, $0 \leqslant r \leqslant r_N(t)$ and $0 \leqslant z \leqslant h(r, t)$, where the density is ρ_c. The subscript N denotes the nose (front) of the intrusion. We argue that the predominant vertical momentum balance in the intruding fluid is hydrostatic and that viscous effects in the horizontal momentum balance are negligibly small. Hence the motion is governed by the balance between pressure and inertia forces in this horizontal direction. The perturbation of the upper free surface introduced by the flow can be neglected when $\epsilon \ll 1$, as assumed here. A deeper justification and discussion of the SW model is presented in [10]. The ultimate test is, of course, the reliability and accuracy of the predicted insights as compared with laboratory and/or numerical experiments. We shall show that the present model indeed provides new insights which agree well with the Navier–Stokes simulation (there are no available laboratory experiments for this problem, to our knowledge).

A relationship between the pressure fields and the height $h(r, t)$ can be obtained. In the motionless ambient fluid, the pressure does not depend on r, and the hydrostatic balances $\partial p_i/\partial z = -\rho_i g$, where $i = a$ or c, and use of (2.4) yield

$$p_a(z,t) = -\rho_o\left[1+\epsilon\left(1-\frac{1}{2}\frac{z}{H}\right)\right]gz + C, \tag{2.6}$$

$$p_c(r,z,t) = -\rho_o(1+\epsilon)gz + f(r,t), \tag{2.7}$$

where C is a constant. Pressure continuity between the ambient and the intrusion on the interface $z = h(r,t)$ determines the function $f(r,t)$ of (2.7) and we obtain

$$p_c(r,z,t) = -\rho_o(1+\epsilon)gz + \rho_o g'\frac{1}{2}\frac{h^2(r,t)}{H} + C, \tag{2.8}$$

and consequently

$$\frac{\partial p_c}{\partial r} = \rho_o g'\frac{h}{H}\frac{\partial h}{\partial r}. \tag{2.9}$$

We note in passing that (2.6)–(2.9), although developed for $z > 0$, are also valid in the $z < 0$ domain. Pressure continuity at $z = -h(r,t)$ and $z = h(r,t)$ are equivalent.

The SW equations of motion are next obtained by z averaging the equations of continuity and radial momentum in the mixed-fluid domain, subject to the inviscid, Boussinesq and thin-layer simplifications; the pressure term is eliminated by (2.9). The results are presented below in dimensionless form.

The dimensional variables (denoted here by asterisks) are scaled as follows

$$\left\{r^*, z^*, h^*, H^*, t^*, u^*, p^*\right\} = \left\{r_0 r, h_0 z, h_0 h, h_0 H, Tt, Uu, \rho_o U^2 p\right\}, \tag{2.10}$$

where

$$U = \left[\frac{\rho_c - \rho_a(z=1)}{\rho_o}h_0 g\right]^{1/2} = (h_0 g')^{1/2}\frac{1}{\sqrt{H}} = \mathcal{N}h_0, \qquad T = \frac{r_0}{U}; \tag{2.11}$$

(to avoid possible confusion, we specify that ρ_a in (2.11) is calculated at the dimensionless $z = 1$). Here, again, r_0 and h_0 are the initial length and half-thickness of the intrusion, U is the typical inertial velocity of propagation of the nose and T is a typical time period for longitudinal propagation over a typical distance r_0. The reference velocity accounts for the fact that the effective driving force is provided by the density difference over the axial dimension of the intrusion. The typical Reynolds number is $Re = Uh_0/\nu$ where ν is the kinematic viscosity.

We emphasize that hereafter the variables r, z, u, t, h, H, p are in dimensionless form unless stated otherwise. The (dimensionless) speed of the dominant wave in the ambient fluid is

$$u_{\text{wave}} = \frac{1}{\pi}H. \tag{2.12}$$

The SW approximation produces a system of equations for the height (or half-thickness) $h(r,t)$ and averaged longitudinal velocity $u(r,t)$. Using these dependent variables, the continuity and momentum equations can be expressed as:

$$\begin{pmatrix} h_t \\ u_t \end{pmatrix} + \begin{pmatrix} u & h \\ h & u \end{pmatrix}\begin{pmatrix} h_r \\ u_r \end{pmatrix} = \begin{pmatrix} -\frac{uh}{r} \\ 0 \end{pmatrix}. \tag{2.13}$$

The characteristics (eigenvalues of the matrix of coefficients) are

$$c_\pm = u \pm h, \tag{2.14}$$

and the corresponding relationships on $\mathrm{d}r/\mathrm{d}t = c_\pm$ are

$$\mathrm{d}h \pm \mathrm{d}u = -\frac{uh}{r}\,\mathrm{d}t. \tag{2.15}$$

For the stratification assumed here the eigenvalues of the matrix of coefficients are real and the set of eigenvectors is full, and hence the system (2.13) is hyperbolic. (Again, we consider only the upper half of the intrusion, $z \geqslant h$, where the half-thickness $h > 0$.)

The boundary conditions are: (1) the obvious $u = 0$ at the center; and, (2) at the nose $r = r_N(t)$

$$u\big(r = r_N(t)\big) = u_N = Fr\left(\frac{h_N}{H}\right)\cdot\frac{h_N}{\sqrt{2}}, \tag{2.16}$$

where the "Froude number" dependency on the relative depth of the nose, h_N/H, is given by the correlation of Huppert and Simpson [12]

$$Fr(h_N/H) = \begin{cases} 0.5\left(\dfrac{h_N}{H}\right)^{-1/3} & (0.075 \leqslant h_N/H \leqslant 1), \\ 1.19 & (0 \leqslant h_N/H \leqslant 0.075, \text{ deep intrusion}). \end{cases} \tag{2.17}$$

This boundary condition, (2.16)–(2.17), has been developed and verified by Ungarish and Huppert [13] and Ungarish [10] as an ingredient of the SW model. A more rigorous justification of the nose condition, in the spirit of the classical analysis of Benjamin [14], is presented by Ungarish [15]. We also recall that Benjamin's prediction for a deep current is $Fr = \sqrt{2}$, which is the maximal attainable value in a Boussinesq system.

The formal assessment of the one-layer model is a difficult task. This is an asymptotic theory with respect to several parameters (e.g., $\epsilon, h_0/r_0, Re^{-1} \to 0$), which uses a steady-state Fr closure for a time-dependent process. The unchanged $\rho_a(z)$ density in the ambient is a quite bold assumption. It is clear that the advancing head lifts some isopycnals from near the bottom to the height of the interface, but since this displaced fluid is kept in a thin layer the influence on the pressure field is expected to be small. A sharp and rigorous estimate of the errors expected for a realistic configuration is therefore not feasible, and order-of-magnitude arguments are used instead. A detailed discussion in this spirit which is relevant to the present problem is presented in [10] Section 2.2. The accepted justification of the model is based mostly on a confidence-building process of critically analyzing the results and performing comparisons with numerical and laboratory experiments. The outcomes for the two-dimensional geometry, reported in [10], provide good support to this formulation. The present study will confirm the applicability and relevance of this model to the propagation of the axisymmetric intrusion.

The 'standard' initial conditions are simply: $r_N = 1$, $u = 0$ and $h = 1$ at $t = 0$. (The $h = 1$ can be changed to reproduce release from a different initial shape, e.g., an ellipsoid $h = \sqrt{1 - r^2}$.)

In general, the solution of this hyperbolic-type initial-value problem is performed by numerical methods. The source term on the right-hand side of (2.15) defies simple analytical solution even during the initial dam-break stage. However, a useful analytical result can be obtained under the assumption that a self-similar behavior develops. This is discussed next.

2.1. Similarity solution

Self-similar results play an important role in the shallow-water analysis of gravity currents in a homogeneous ambient (see Grundy and Rottman [16], Gratton and Vigo [17], Hogg et al. [18], and Slim and Huppert [19]). Ungarish [10] presented a similarity solution for a deep intrusion in the stratified ambient in a two-dimensional geometry. In this case the propagation of the nose obeys $x_N(t) \sim t^{1/2}$ (at large t), see Appendix A.

We sought a self-similarity solution to the system of SW governing equations and boundary conditions, for a deep intrusion and large values of t. At this stage we do not impose initial conditions. If the intrusion is deep it is justified to assume that $Fr = \text{const}$ (= 1.19 in the present formulation, see (2.17)).

We found that the abovementioned system of equations and boundary conditions (see (2.13) and (2.16)), when Fr is constant, is satisfied by

$$r_N(t) = K(t+\gamma)^{1/3}, \quad h(y,t) = \dot{r}_N \sqrt{2}\left(y^2 - y_1^2\right)^{1/2}, \quad u(y,t) = \dot{r}_N y, \tag{2.18}$$

where the upper dot means differentiation with respect to t. Here

$$y = \frac{r}{r_N(t)}$$

is the stretched radial coordinate which maps the radial domain $[0, r_N(t)]$ into $[0, 1]$,

$$y_1 = \sqrt{1 - \frac{1}{Fr^2}}, \tag{2.19}$$

and K and γ are constants which represent the initial conditions, see below. Obviously, K and $(t+\gamma)$ must be positive for physically-acceptable results.

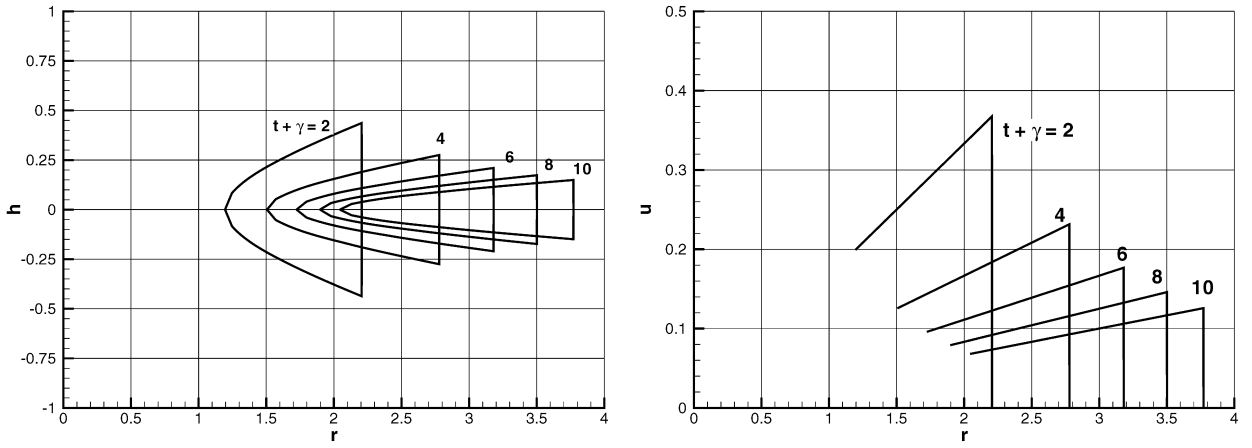

(a) (b)

Fig. 2. Self-similar shape of interface and velocity for an intrusion of volume $\mathcal{V} = 0.5$ at various times $t + \gamma$. The 'negative' h is the mirror image of the calculated h.

The linear variation of u with y is a common feature of self-similar propagation. On the other hand, the dependency of h on $(y^2 - y_1^2)^{1/2}$ contributes a novel, non-expected feature. Since $y_1 > 0$ for $Fr > 1$ (as assumed here in accordance with practical and theoretical evidence), and h is a real-valued non-negative variable, we realize that the solution (2.18) is physically valid only in the domain $y_1 \leqslant y \leqslant 1$. (In the present case, for $Fr = 1.19$, we obtain $y_1 = 0.54$.) Moreover, we note that $h(y_1) = 0$. In other words, in the self-similar stage the intrusion is a ring of mixed fluid embedded in the original ambient fluid. The inner radius, $r_1(t) = y_1 r_N(t)$, is slightly larger than half the outer radius in the present case. The thickness of the intrusion decreases continuously to zero as $y \to y_1^+$. The typical behavior of the shape of the resulting self-similar intrusion is illustrated in Fig. 2.

The positive constant K is determined by volume continuity considerations. Conservation of the initial volume, $\mathcal{V}$, of the intruding fluid can be expressed as

$$\int_{r_1(t)}^{r_N(t)} h(r,t) r \,\mathrm{d}r = \dot{r}_N r_N^2(t) \int_{y_1}^{1} \sqrt{2}\left(y^2 - y_1^2\right)^{1/2} y \,\mathrm{d}y = \mathcal{V}. \tag{2.20}$$

Substituting $r_N(t) = K(t+\gamma)^{1/3}$ yields, after some algebra,

$$K = 3Fr\left[\frac{\mathcal{V}}{3\sqrt{2}}\right]^{1/3}, \tag{2.21}$$

where, again, $\mathcal{V}$ is the constant volume of the intrusion (per unit azimuthal angle). For the present value of $Fr = 1.19$ we obtain: (a) for the 'standard' initial cylinder of mixed fluid $\mathcal{V} = 1/2$, and hence $K = 1.750$; (b) for an initial ellipsoid of mixed fluid $\mathcal{V} = 1/3$, and hence $K = 1.529$.

Finally, the constant γ is used to compensate for the 'virtual origin' deficiency of the self-similar solution. Indeed, in the physical system at $t = 0$ the velocity is $u = 0$, and the geometry of the dense fluid in the lock is given. These initial conditions cannot be imposed on (2.18). However, the real time coordinate can be shifted by the parameter γ to achieve matching with the developed flow produced by the real initial behavior of the intrusion. In the present lock-release case a reasonable matching time is $t = 5$ (measured from the release). This time interval is expected to encompass the establishment and decay of the initial dam-break slumping motion by the backward-forward motion of the characteristics in the initially stationary mixed fluid. We shall show below, using the SW initial-value finite-difference solutions, that this is indeed a proper choice, and yields $\gamma \approx -1.60$.

Another useful observation concerning the similarity solution (2.18) is that

$$c_- = u - h > 0 \quad \text{for } y < \sqrt{2} y_1. \tag{2.22}$$

This indicates that information from the nose cannot be propagated back into the trailing edge and disturb the tendency of h to decay to 0.

The importance of the viscous forces during the self-similar propagation can be estimated using (2.18). We assume that the viscous and inertia terms (per unit volume) are proportional to $\nu u^*/(h^*)^2$ and $u^*(\partial u^*/\partial r^*)$, respectively, in dimensional form. We obtain

$$\frac{\text{Inertia}}{\text{Viscous}} \approx \frac{Uh_0}{\nu}\left(\frac{h_0}{r_0}\right) r_N^{-7}. \tag{2.23}$$

Since the typical $Re = Uh_0/\nu \approx 10^5$ and $h_0/r_0 < 1$, the inviscid model is expected to be valid for $r_N < 5$ only.

We recall that in a non-stratified ambient fluid the similarity behavior of an axisymmetric intrusion/current (see Grundy and Rottman [16], Bonnecaze et al. [20]) displays: (a) propagation with $r_N(t) \sim t^{1/2}$; (b) interface profile $\dot{r}_N^2[Fr^{-2} + 0.5(y^2 - 1)]$ for $0 \leqslant y \leqslant 1$; and (c) $c_- < 0$ for $y < (2/Fr^2 - 1)$. Thus, in the non-stratified ambient the thickness of the self-similar current is non-zero for all $r \geqslant 0$. In this case the ratio of the inertia to viscous terms behaves like r_N^{-6}, see Huppert [21]. (We note in passing that for $Fr > 2$ the interface profile attains negative values near the center. This type of behavior for large Fr has been pointed out by Gratton and Vigo [17]. Formally, this limits the applicability of the solution to some $y \geqslant y_2 > 0$ when $Fr > \sqrt{2}$. However, since for the Boussinesq currents considered here such values of Fr are physically impossible, this limitation can be ignored.)

As expected, the intrusion in the stratified ambient spreads out slower, with $t^{1/3}$, and the dominance of the inertia terms decays faster, with r_N^{-7}. However, the striking novel feature of the present self-similar case, is the appearance of a clear inner domain, while the whole volume of the intrusion is confined to an annular domain with a fixed ratio between the inner and outer radii, see Fig. 2. This structure is also very different from the two-dimensional stratified case (see Appendix A).

3. Results and comparisons

3.1. Deep ambient

The first task is to solve the development from the initial release and verify whether and when the abovementioned stage of self-similar propagation is approached. This investigation is also expected to provide the proof that the peculiar similarity shape is indeed attainable from a simple, physically feasible, lock-release initial condition.

We solved the initial-value SW problem (again, with $u = 0$ and $h = h(r)$ in $0 \leqslant r \leqslant r_N = 1$ at $t = 0$) by a finite-difference two-step Lax–Wendroff scheme. The discretization was performed on the conservation form of (2.13) (see [22–25]). The typical grid has 300 intervals in $[0, r_N]$ and the typical time step is 1×10^{-3}. The convergence and accuracy of the finite-difference results presented here has been confirmed by numerous numerical tests (e.g., repeated runs with different grids, Courant numbers and artificial viscosity coefficients).

The 'standard' problem is the release of a cylinder of mixed fluid, i.e., $h = 1$ for $0 \leqslant r < 1$, $t = 0$. Pertinent results are presented in Fig. 3. Here the initial depth ratio is $H = 9$. This provides, from the beginning, a sufficiently deep 'nose' and hence a constant $Fr = 1.19$, see (2.17). (We verified that identical results were obtained for $H = 7$ and $H = 20$.) During the initial phase of propagation (see $t = 1$) the shape resembles the behavior of the dam-break problem: the height of the interface of the fluid propagating from the lock (the 'head') is about half the initial height, while in the lock domain (the 'tail') the interface becomes negatively-inclined due to a backwardly propagating relaxation wave. However, the radial velocity in the lock region increases with r and reaches a maximum at $r \approx 1$. This is a result of the cylinder-geometry constraint on the characteristic balances. Consequently, fluid is quite quickly drained from the 'tail' into the $r > 1$ domain. At $t = 3$, the 'tail' contains less than 10% of the initial volume. It is clearly seen that the mixed fluid, released from rest in the cylinder lock, has the tendency of to evolve into the ring-shape of the self-similar analytical prediction displayed in Fig. 2. The sharp difference to the corresponding rectangular current, of both h and u profiles, is illustrated by Fig. 10 in Appendix A. To strengthen the insights into the propagation of a deep intrusion, we also considered the release of an initial ellipsoid volume of mixed fluid, i.e., $h = \sqrt{1 - r^2}$ for $0 \leqslant r < 1, t = 0$. Fig. 4 shows that the essential propagation is like in the previous 'standard' problem. The initial spread is slightly delayed by the fact that the height of the nose must develop from zero, but the tendency to the similarity shape at $t > 3$ is evident.

Now we calculate the value of γ by matching, at $t = 5$, the numerically computed r_N with the similarity form $K(t + \gamma)^{1/3}$, where K is known as specified above. The result is $\gamma = -1.53$ for the cylinder and -1.63 for the ellipsoid. Using this outcome, we compare the numerical and similarity predictions of radius and velocity of propagation

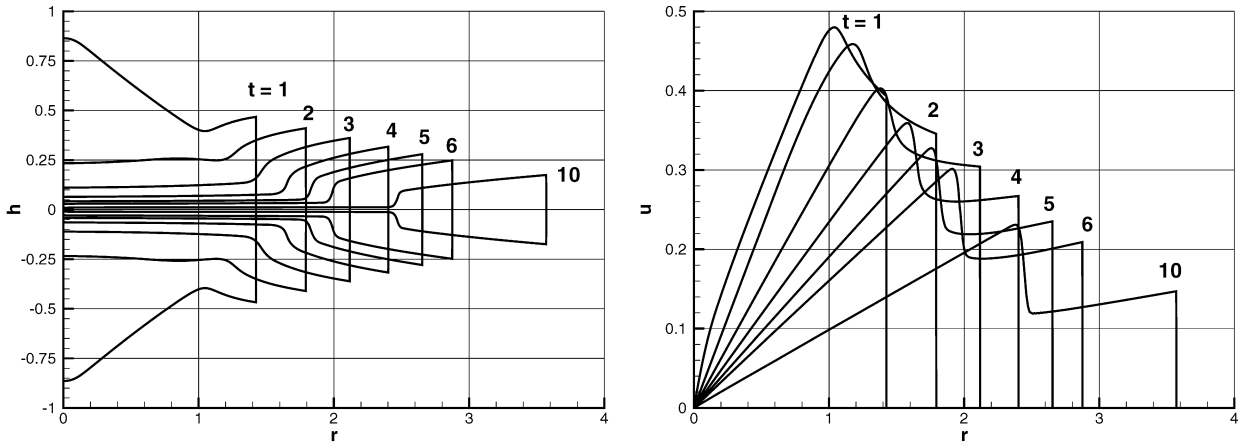

(a) (b)

Fig. 3. SW predictions for release of a deep intrusion ($H \geqslant 7$) from rest. The initial volume is a cylinder ($h = 1$). Profiles of thickness and u as functions of r for various t.

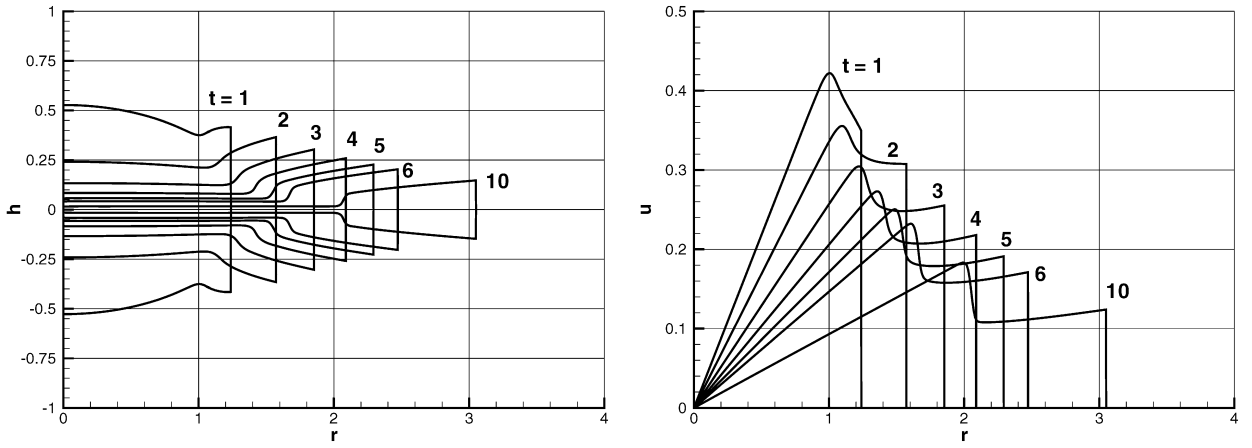

(a) (b)

Fig. 4. As in the previous figure, but the initial volume is an ellipsoid ($h = \sqrt{1 - r^2}$).

over a wide range of t, see Fig. 5. The observed agreement is good. We verified that this trend is maintained up to $t = 100$ (to be specific, we found that for $t > 4.5$ the discrepancy is less than 3.2% for the radius, and about 6% for the velocity). A sharper description of the large-time behavior requires a specially designed code. This investigation is currently underway.

The behavior of the thin tail turns out to be also quite interesting. We see in Figs. 3, 4 that for $t \geqslant 2$, the interface of the tail is horizontal and the corresponding velocity increases linearly with r (as first approximations). This feature can be explained analytically as follow. Consider the equations of motion (2.13) subject to the boundary condition $u = 0$ at $r = 0$. For $h(r, t)$ and $u(r, t)/r$ we seek approximations of the form $f_0(t) + f_1(r, t)$ under the assumption that $|f_1|/|f_0| \ll 1$ for large t. Substitution of the corresponding expansions into (2.13) yields, after some algebra, the leading terms

$$h(r, t) = \frac{C_1}{(t + C_2)^2}, \qquad u(r, t) = \frac{1}{t + C_2} r, \tag{3.1}$$

where C_1, C_2 are constants which represent some (as yet unspecified) initial conditions. We note that (3.1) is actually an exact solution of (2.13). Formally, this can also be referred to as a self-similar inner-region behavior. An order of magnitude consideration shows that C_1, C_2 are positive and of order unity.

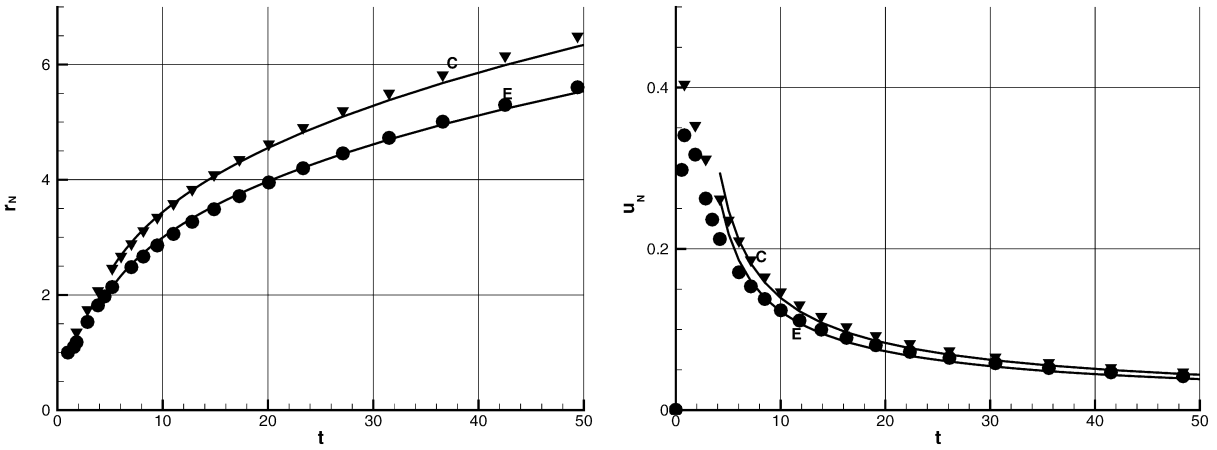

(a) (b)

Fig. 5. Comparison of similarity (line) and initial-value results (symbols) for a cylinder (C) and ellipsoid (E) initial shape.

The behavior (3.1) of the thin tail provides additional and supportive insight into the development of the major similarity shape from realistic initial conditions. An inspection of the characteristic speeds $c_\pm$ indicates that the tail is able to spread out quickly. We therefore expect that, for large t, this tail extends from the axis to the position $r_1 \approx y_1 K t^{1/3}$ where the similarity profiles (2.18) starts. (For simplicity, we discard the constants γ and C_2 in the present discussion.) First, combining this r_1 with $h \sim t^{-2}$, we infer that the volume of fluid in the tail, which is (approximately) $0.5 r_1^2 h$, decays like $t^{-4/3}$ for large t. Second, substituting this r_1 into (3.1), we obtain $u(r_1, t) = y_1 K t^{-2/3}$ for large t in the tail. On the other hand, the similarity solution (2.18) predicts that u varies from $(1/3) y_1 K t^{-2/3}$ (at r_1) to $(1/3) K t^{-2/3}$ (at r_N). This means that the value of u is expected to reach the maximum in the tail (recall that $y_1 = 0.54 > 1/3$). Third, we notice that in the region about r_1 the value of $c_- = u - h$ is positive. This implies that information from the head is not propagated into the tail, and hence the behavior (3.1) for $y \leqslant y_1$ remains unaffected from the connection with the self-similar region (2.18). These predictions are consistent with the u profiles displayed in Figs. 3, 4. Indeed, at a given time, u increases linearly with r until about the position where the thin tail ends. There u reaches the maximum. Then a sharp decrease of u with r occurs, followed by, again, a liner increase with r. These features are observed for both the cylinder and ellipsoid initial volume.

Additional details of the dependencies predicted by (3.1) were verified and confirmed by comparisons with the SW solutions. The fit to the numerical Lax–Wendroff results yields: $C_1 = 1.19$, $C_2 = 0.194$ for the cylinder; and $C_1 = 0.815$, $C_2 = 1.946$ for the ellipsoid. However, the details of the tail are rather of academic importance, concerning the transition phase to the similarity behavior. Practically, the tail domain is expected to be of little importance to the flow-field after the formation of the main self-similar ring (say, $t > 4$). We must also keep in mind that, in a real flow, the decay of thickness, volume and energy in the tail is augmented by mixing and friction. Consequently, the present inviscid immiscible SW description of the tail may lose physical relevance in a quite early stage. Indeed, repeating the foregoing order-of-magnitude estimates using the flow-field (3.1), we find that in the tail domain

$$\frac{\text{Inertia}}{\text{Viscous}} \approx \frac{U h_0}{\nu}\left(\frac{h_0}{r_0}\right) t^{-5} \approx \frac{U h_0}{\nu}\left(\frac{h_0}{r_0}\right) K^{15} r_N^{-15}, \tag{3.2}$$

where K is the coefficient of the similarity propagation (2.18) (this constant is included here because it contributes a factor of about 10^3 to the above ratio).

The main conclusions are: (1) The self-similar behavior (2.18) is indeed approached by the SW initial-value lock-release problem of a deep intrusion, for practical initial volumes. The adjustment time is about $t = 4$ during which propagation to $r_N \approx 2.5$ occurs. (2) In the inner side of the similarity ring there is a residual horizontal layer of mixed fluid whose thickness decays like t^{-2} (for $t > 2$). (3) The thin tail layer becomes affected by viscous effects at a quite early stage of propagation (say, at $t = 4$ and $r_N = 2.5$) but the self-similar major domain maintains the inviscid behavior for a substantially longer time and radius of propagation (say, $t = 30$ and $r_N = 5$).

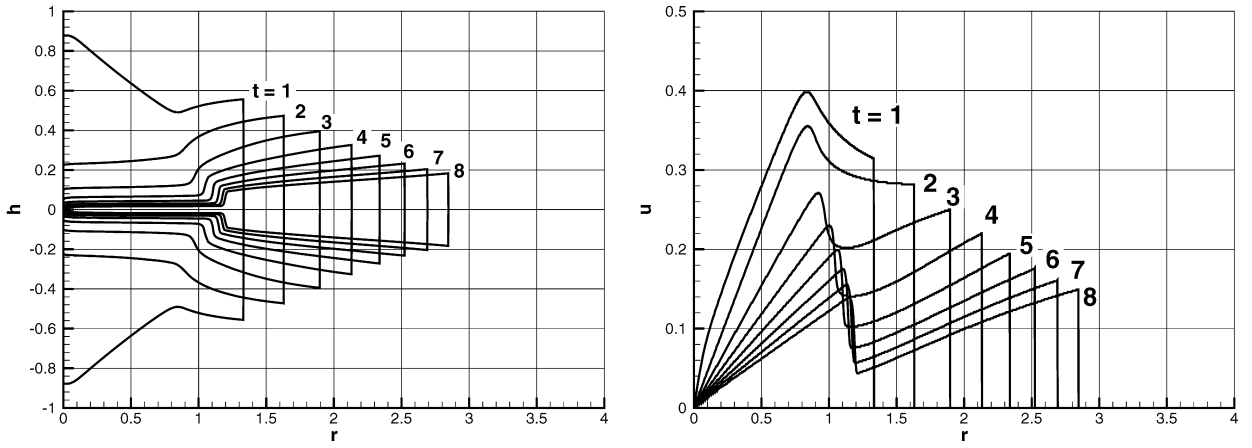

(a) (b)

Fig. 6. SW predictions for $H = 2.27$. Profiles of h and u as functions of r for various t.

3.2. $H = 2.27$

Here the SW results are verified by a 'numerical experiment'. The configuration discussed here has been chosen because it has a realistic counterpart in the two-dimensional (rectangular) geometry. The relevant two-dimensional experiment was performed by Amen and Maxworthy [5], Run no. 117 (salt water, $h_0 = 6.16$ cm, $\mathcal{N} = 0.57$ s^{-1}, $h_0/x_0 = 0.33$, where x_0 is the length of the lock). The Navier–Stokes and SW simulations of this experiment were presented by Ungarish [10]. For the convenience of the reader, some of these results are duplicated here in Appendix A). The comparison of the present axisymmetric results with the previous two-dimensional flow-field is expected to enhance our understanding of these problems.

The SW results are presented in Fig. 6. We observe that for $t \geqslant 3$ the motion of this intrusion resembles the similarity behavior, cf. Fig. 2. In particular, the volume is concentrated in an annular domain (with a thin tail whose thickness decays with time). The tail region develops a horizontal interface for $t > 2$, where next $h \propto t^{-2}$. The velocity in the intrusion, u, displays, again, two regions of linear increase with r, with a quite sharp drop of value in a transition region about the inner radius of the annulus. We infer that the main qualitative features of the SW similarity solution, derived for a deep intrusion, are valid also for release at moderate depths ($H = 2.27$ here).

The Navier–Stokes simulations were performed for a counterpart configuration, as follow. The numerical, axisymmetric, tank has the outer radius $r_w = 4$ and (half-)height $H = 3$. This r, z domain was covered by a 260×180 unstretched mesh. We used $\epsilon = 4.65 \times 10^{-3}$ and $Re = 2.3 \times 10^4$. Rigid boundary conditions were applied at the bottom and outer cylindrical wall, and no-stress and regularity conditions at the axis $r = 0$. It was assumed that the top is a free-slip flat surface. A description of the code essentials is given in [10]; here we used an extension for a cylindrical fully axisymmetric flow-field (i.e., the spatial dependence is on r, z only). This code was validated by: (a) standard numerical verifications of repeating runs with grid and time-step variations; and (b) comparisons with available experimental data concerning propagation in two-dimensional configurations (see [10,26]). We estimated that the present r_w is sufficiently large for preventing interference between the intrusion and the reflected wave during the time intervals of interest here ($t < 7$), and that the grid is sufficiently fine for resolving the expected features. Initially, the current in the lock is covered by 65 radial and 79 axial grid intervals. At the maximal propagation considered here, we found that there still are about 20 axial grid intervals in the main nose region of the intrusion. The main objectives of our simulation are to confirm the predictions of the SW model (in particular concerning the appearance of the ring structure), and to check if and how this is affected by the wave-head possible interaction. The rich and smooth details of the computed flow fields presented below, and in particular the clear-cut differences between the results in the axisymmetric and two-dimensional geometries, indicate that the numerical resolution was satisfactory.

Density contours of the NS solution are shown in Fig. 7. The nose of the intrusion is indicated by the large $>$ (this is the foremost position of the domain with scaled density $\phi = 0.5$; the contours 0.51 and 0.49 embed this domain). The NS simulations, performed for the full domain $-H \leqslant z \leqslant H$ (as detailed in [10]), confirm the SW assumption of

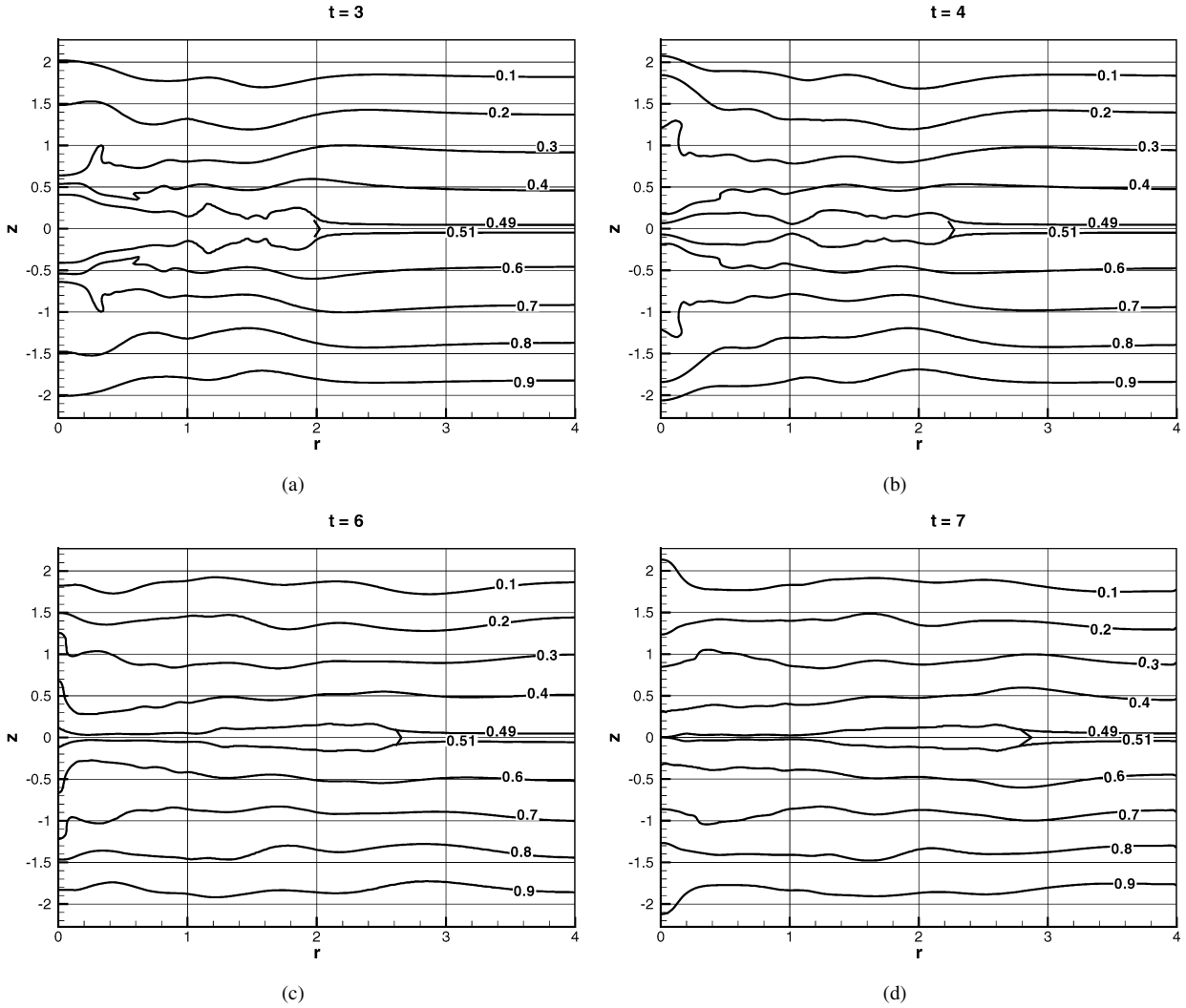

Fig. 7. Density contour lines at various times, NS computations, for axisymmetric configuration with $H = 2.27$, $h_0/x_0 = 0.33$. The nose is marked by $>$.

symmetry about $z = 0$. Some small deviations appear near the boundaries because in the NS simulations free slip and no-slip condition are applied at the top and bottom, respectively, to reproduce a real experimental tank.

We observe that at $t = 6$ in the central domain, $r < 1.1$ (approximately), the intrusion is very thin, and most of the mixed-fluid volume is concentrated at larger radii. This shape is more pronounced at $t = 7$. We think that this behavior confirms the SW predictions concerning both the (a) peculiar similarity shape (see Fig. 2), and (b) the thin tail in the inner region. When the NS-simulated layer of intruding fluid becomes very thin, viscous effects are expected to enter into the balance and hinder the motion in this region. Actually, the SW approximation is also expected to lose validity at the matching point $y = y_1+$ because $\partial h/\partial y \to \infty$ there, see (2.18). We mention in passing that a similar thin residual layer is also expected to develop in a laboratory experiment.

The isopycnals in the ambient above and below the intrusion display a wavy structure. The typical wavelength (scaled with r_0) is expected to be $2\pi(h_0/x_0)u_N \approx 0.7$ during the initial stages of motion. This is consistent with the NS results. However, at the present state of knowledge, it is difficult to predict the amplitude of these waves. The order of magnitude is implied by the displacement the neutral buoyancy line by the intruding nose, which is expected to be $\pm h_N \approx 0.4$ during the initial stages of motion. Since both u_N and h_N decay with time, and the bulk of the intrusion is affected by the backward moving 'dam break' expansion wave, the resulting amplitude of the displaced isopycnals is quite irregular. The question how to quantify the effect of these displacements into a SW model error is left to

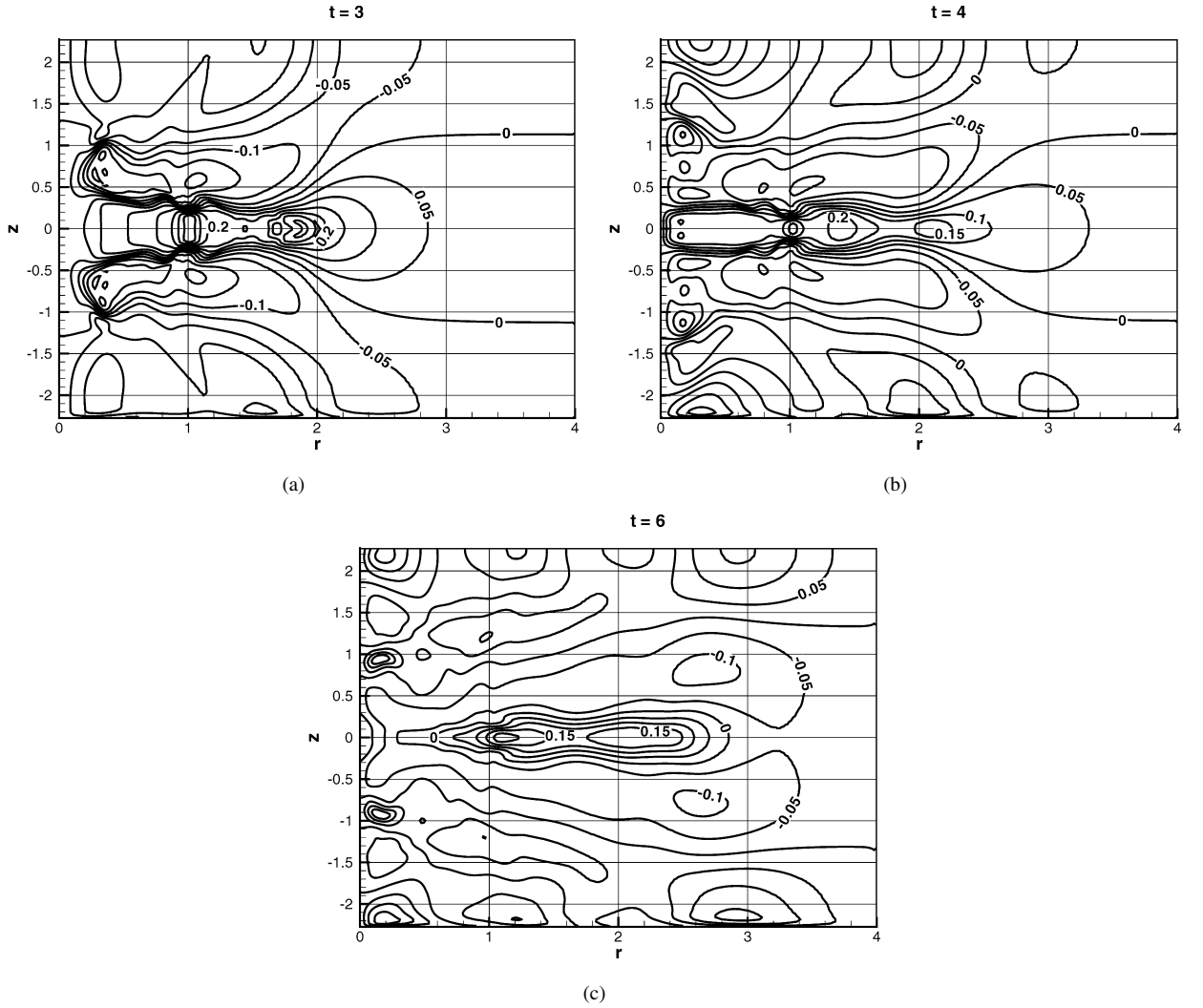

Fig. 8. u contour lines at various times, NS computations, for axisymmetric configuration with $H = 2.27, h_0/x_0 = 0.33$.

further research. A propagation of the density perturbation ahead of the nose is also observed. However, the density perturbations induced by the leading wave are small (during the time considered here, at least). This supports the SW model assumption that the ambient in front of the intrusion maintains the initial $t = 0$ structure, in spite of the fact that the propagation is sub-critical.

It is interesting to note that in the present axisymmetric case there is almost no interaction between the waves and the head of the current. This is in sharp contrast with the two-dimensional counterpart, where a strong interaction appeared from $t \approx 5$ in both the numerical and experimental data. The possible explanation is the very different geometry of the head. In the axisymmetric case the head carries a significant portion of the total volume, while in the two-dimensional case a significant volume is contained in a thick and long tail (see Fig. 11).

The behavior of the velocity field is illustrated by contour lines of u in Fig. 8. The NS results display the difference between the tail and front of the mixed-fluid region, which has been indicated by the SW profiles. The radial velocity is large near $r = 1$ and near the nose, as predicted by the SW approximation. As expected, a return flow develops in the ambient between the boundaries and the head of the intrusion. This flow is strongly z-dependent and therefore it would be difficult to incorporate it in a simple two-layer SW model.

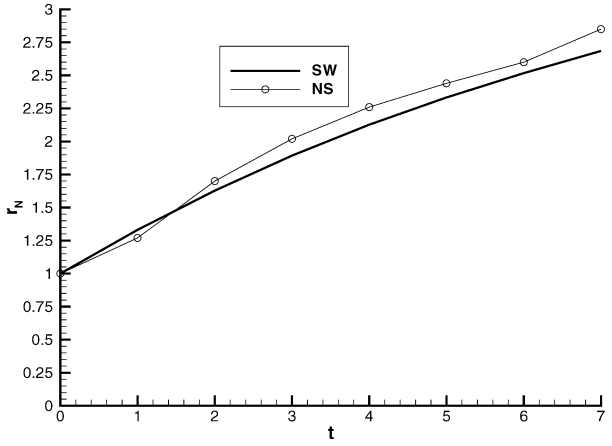

Fig. 9. Radius of propagation as a function of t for axisymmetric $H = 2.27$ configuration, NS and SW results.

The radius of propagation as a function of time is displayed in Fig. 9. The agreement between the NS and SW predictions is very good. The small oscillation of the NS result can be attributed to the influence of the internal waves. Again, this turns out to be a small effect.

The overall conclusion is that the SW model is an insightful and fairly accurate approximation to the real flow-field, at least for the initial times considered here.

Finally, we compare the speed of propagation of the axisymmetric intrusion with that of the two-dimensional rectangular counterpart. The balance along a forward-moving characteristic, see (2.15), indicates that the initial speed (at $t = 0^+$) is the same in both cases, but afterwards the axisymmetric intrusion moves more slowly. This is a result of the negative source term in (2.15) which expresses the divergence of the radial flow in the cylindrical geometry (this term is obviously zero in the rectangular case). It was shown in [10] that the rectangular two-dimensional propagation is always subcritical (i.e., $u_N < u_{\text{wave}}$ given by (2.12)). We conclude that the speed of propagation of the axisymmetric intrusion is also always subcritical.

4. Concluding remarks

The propagation of a cylindrical axisymmetric intrusion (mixed fluid) of a given volume released at the neutral buoyancy level in a stratified ambient was considered. We used a new analysis, based on a one-layer shallow-water (SW) closed formulation, and backed by numerical solutions of the Navier–Stokes (NS) equations. Predictions were obtained for realistic geometries, initial and boundary conditions. The theory does not rely on adjustable constants or predetermined shapes. This is a useful extension of the two-dimensional counterpart problem presented by Ungarish [10].

The SW theory predicts that, after an initial propagation to about 2.5 times the initial radius, the intrusion attains a self-similar behavior. In this stage the spread is with $t^{1/3}$ and the bulk of mixed fluid is in a ring of fixed ratio of the inner to outer radii (of about one half). Inside the inner radius of the ring there is a thin residual layer (disk) of mixed fluid, whose thickness decreases like t^{-2}. The speed of propagation of the nose (front) of the intrusion is sub-critical in all stages of propagation.

The NS simulations confirm the SW predictions. These results incorporate the effect of the internal gravity waves, which is ignored in the SW approximation. It turns out that the wave-head interaction in the axisymmetric geometry is quite insignificant, in contrast to the two-dimensional rectangular counterpart problem.

The present results provide additional credence to the novel stratified-ambient one-layer SW model. The good agreement with the NS results concerning the ring-shape and the radius of propagation as a function of time cannot be just coincidence. This adds to the good performances observed in the rectangular geometry. In our opinion, this is a clear-cut indication that the components of the model, although not rigorously justified theoretically, capture well the essentials of the underlying physical mechanisms. This conclusion applies to the combination of: (1) the hyperbolic volume and momentum governing equation (2.13); (2) the *Fr* correlation (2.17) (taken "off the shelf" from the knowledge on the homogeneous gravity current); and (3) the nose driving-force conjecture (2.16). All these

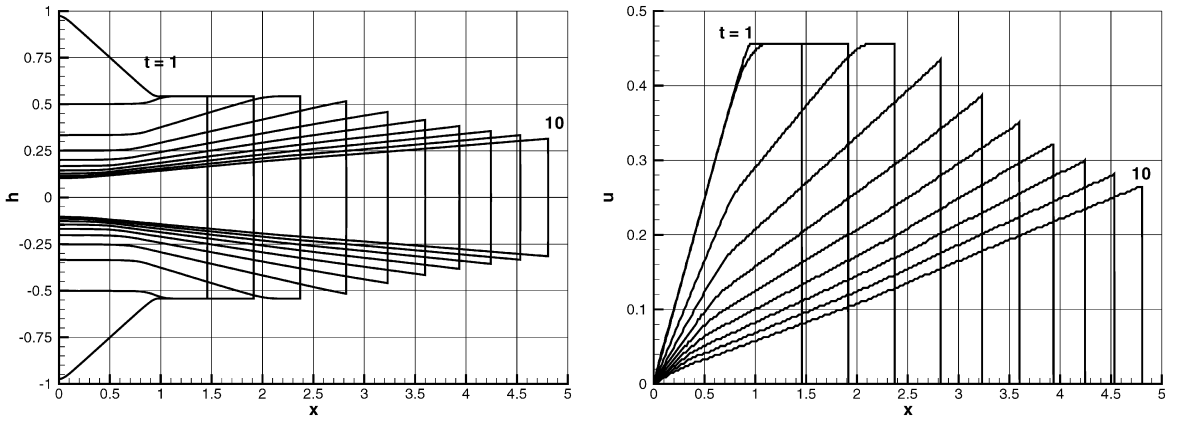

Fig. 10. SW predictions for release from rest of a two-dimensional rectangular deep intrusion ($H \geqslant 7$). The initial volume is a rectangle ($h = 1$). Profiles of h and u as functions of x for various t [1 (1) 10].

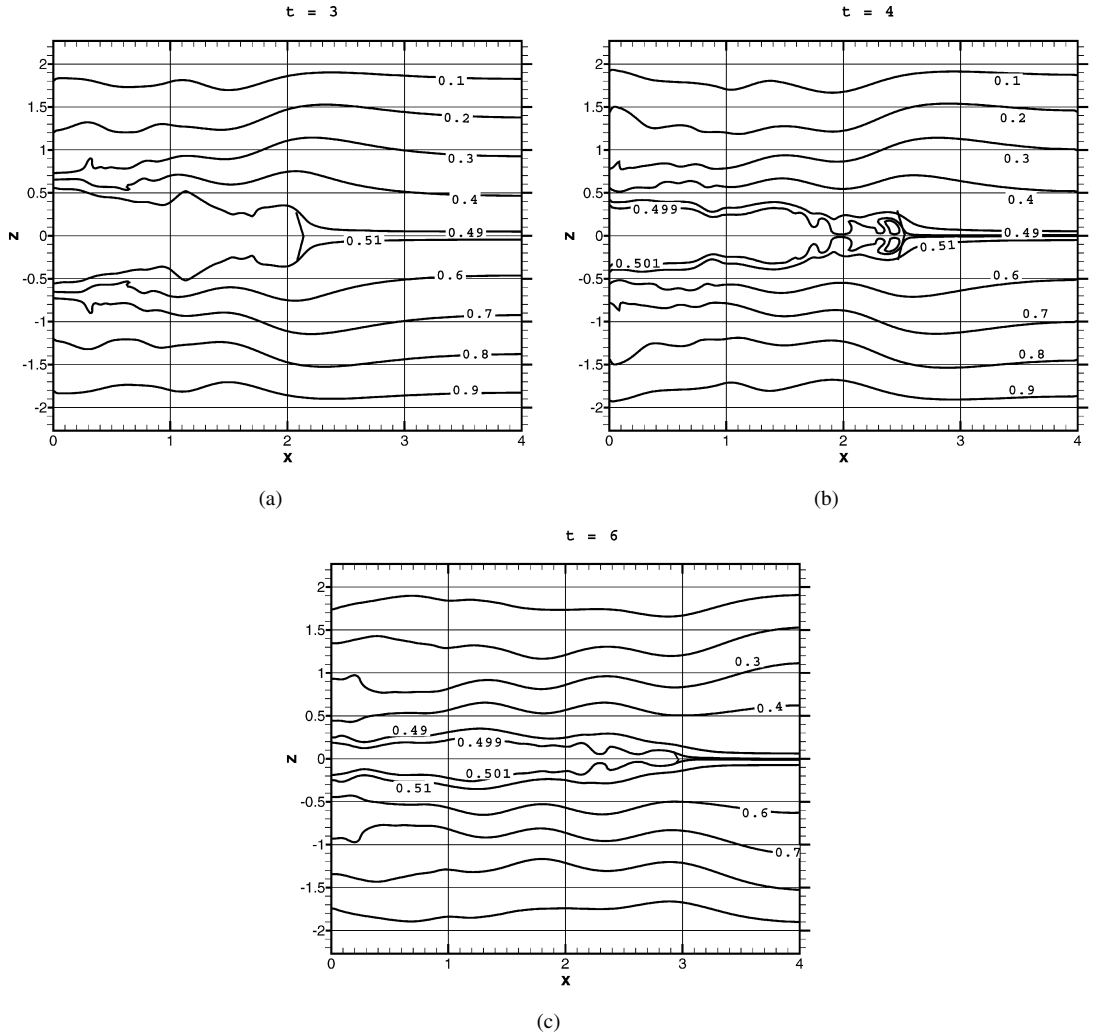

Fig. 11. Density contour lines at various times, NS computations, for rectangular configuration with $H = 2.27$, $h_0/x_0 = 0.33$ (simulation of run 117 of Amen and Maxworthy). The nose is marked by $>$.

components are necessary for the accurate description of the motion in both the initial and developed (self-similar) stages. Moreover, it was shown that the present SW model is a versatile and robust tool which is amenable to various extension (e.g., coordinate systems and the initial shape of the released volume). The model admits useful analytical similarity solutions and can be efficiently solved by finite-difference classical schemes. However, after a spread to a relatively large radius the intrusion is expected to become thin and slow. At this stage, in a real fluid, the effects of viscosity, mixing and wave interaction are expected to become dominant. The buoyancy-driven intrusion is expected to evolve into a wave, see, for example, Manasseh et al. [27]. This requires a separate investigation.

We showed that the ratio of the inertia to viscous terms in the horizontal momentum balance decays with r_N^7 (in the non-stratified counterpart, the result is r_N^6). This poses quite a strong limitation on the applicability of the inviscid theory, and provides strong motivation to the investigation of the viscous case. This is left for future study.

The lack of experimental data prevents sharper conclusions about the insights provided by the present theory. We hope that the present study will provide the background, guidelines and the motivation for the laboratory experiments on this problem.

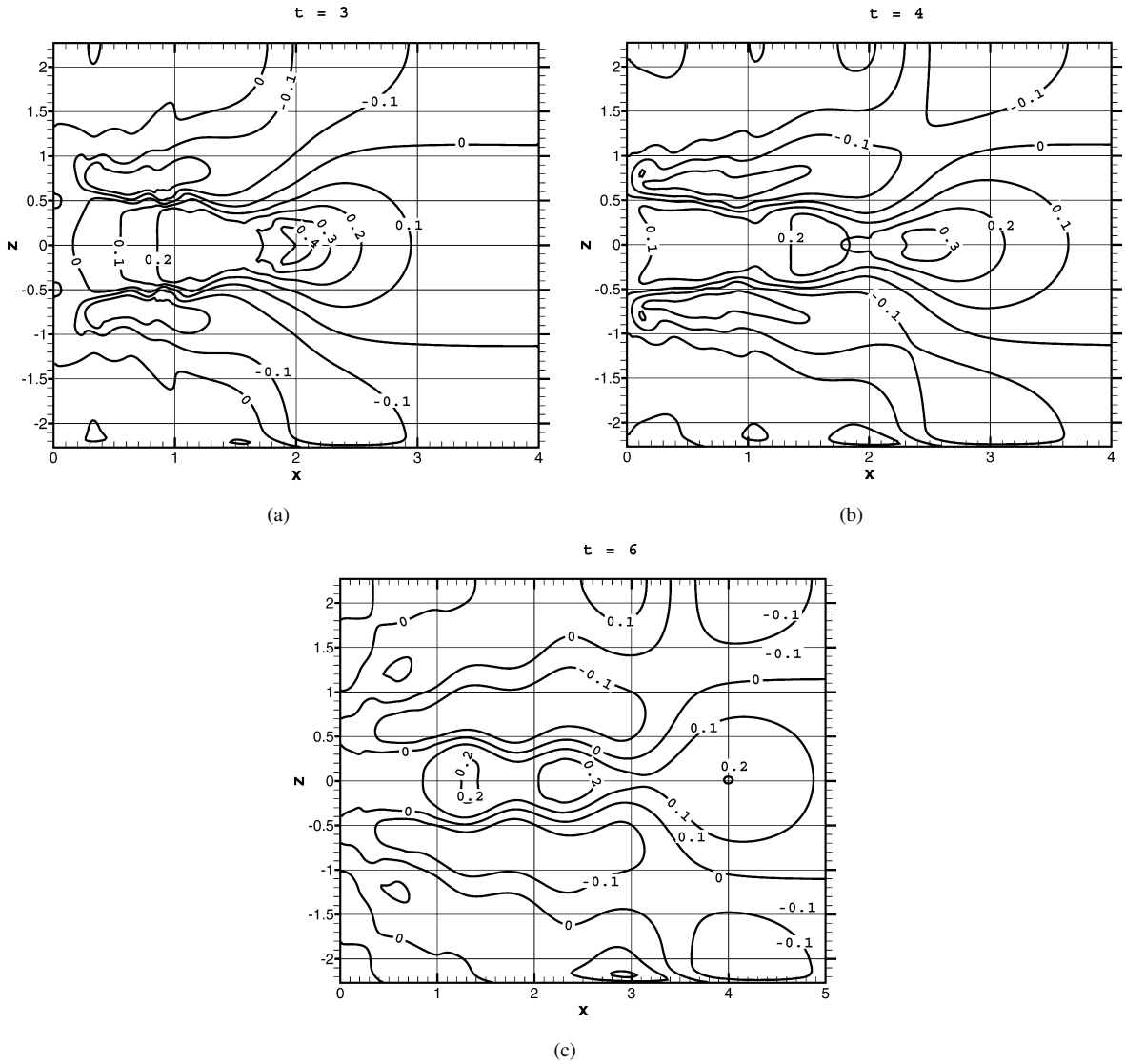

(a) (b) (c)

Fig. 12. u contour lines at various times, NS computations, for rectangular configuration with $H = 2.27$, $h_0/x_0 = 0.33$ (simulation of run 117 of Amen and Maxworthy).

Appendix A. Two-dimensional results

For comparison, some results for the two-dimensional rectangular configuration, discussed in detail by [10], are presented in this appendix. The radial coordinate r is changed to the Cartesian x and r_0 to x_0 (including in the scaling (2.10)–(2.11)). The curvature source right-hand-side terms in (2.13) and (2.15) vanish.

The similarity solution for a deep intrusion is

$$x_N(t) = K(t+\gamma)^{1/2}, \quad u = \dot{x}_N(t)y, \quad h = \dot{x}_N(t)\left(b^2 + y^2\right)^{1/2} \quad (0 \leqslant y \leqslant 1), \tag{A.1}$$

where $y = x/x_N(t)$ is the stretched horizontal coordinate, K and γ are constants,

$$b^2 = \frac{2}{Fr^2} - 1, \tag{A.2}$$

and the upper dot means differentiation in time. Here $K = 1.537$ for a rectangle lock and 1.362 for a cylinder lock $h = (1-x^2)^{1/2}$; $\gamma \approx -0.6$ in both cases. We recall that $Fr \leqslant \sqrt{2}$ in the cases under consideration. The ratio of inertia to viscous forces decreases with x_N^4.

The SW propagation of a deep ($H \geqslant 7$) intrusion released from a rectangle lock ($h = 1$) is illustrated in Fig. 10.

Some NS density- and u-contours results of the rectangular configuration $H = 2.27$ are shown, Figs. 11, 12, to contrast with the axisymmetric counterpart. In particular, we wish to emphasize the differences in: (1) the structure of the head and tail regions of the intrusion; (2) the wave-head interaction at $t = 4$ and 6; (3) the dependency of u on r in the intrusion domain.

References

[1] J.E. Simpson, Gravity Currents in the Environment and the Laboratory, Cambridge University Press, 1997.
[2] J. Wu, Mixed region collapse with internal wave generation in a density-stratified medium, J. Fluid Mech. 35 (1969) 531–544.
[3] T.W. Kao, Principal stage of wake collapse in a stratified fluid: Two-dimensional theory, Phys. Fluids 19 (1976) 1071–1074.
[4] P.C. Manins, Mixed region collapse in a stratified fluid, J. Fluid Mech. 77 (1976) 177–183.
[5] R. Amen, T. Maxworthy, The gravitational collapse of a mixed region into a linearly stratified fluid, J. Fluid Mech. 96 (1980) 65–80.
[6] K.M. Faust, E.J. Plate, Experimental investigation of intrusive gravity currents entering stably stratified fluids, J. Hydraulic Res. 22 (1984) 315–325.
[7] F. de Rooij, Sedimenting particle-laden flows in confined geometries, PhD thesis, DAMTP, University of Cambridge, 1999.
[8] G. Ivey, S. Blake, Axisymmetric withdrawal and inflow in a density-stratified container, J. Fluid Mech. 161 (1985) 115–137.
[9] C. Lemckert, J. Imberger, Axisymmetric intrusive gravity currents in stratified reservoirs, J. Hydraulic Engrg. 119 (6) (1993) 662–679.
[10] M. Ungarish, Intrusive gravity currents in a stratified ambient – shallow-water theory and numerical results, J. Fluid Mech. 535 (2005) 287–323.
[11] P.G. Baines, Topographic Effects in Stratified Flows, Cambridge University Press, 1995.
[12] H.E. Huppert, J.E. Simpson, The slumping of gravity currents, J. Fluid Mech. 99 (1980) 785–799.
[13] M. Ungarish, H.E. Huppert, On gravity currents propagating at the base of a stratified ambient, J. Fluid Mech. 458 (2002) 283–301.
[14] T.B. Benjamin, Gravity currents and related phenomena, J. Fluid Mech. 31 (1968) 209–248.
[15] M. Ungarish, On gravity currents in a linearly stratified ambient: a generalization of Benjamin's steady-state propagation results, J. Fluid Mech. 548 (2006) 49–68.
[16] R.E. Grundy, J. Rottman, The approach to self-similarity of the solutions of the shallow-water equations representing gravity current releases, J. Fluid Mech. 156 (1985) 39–53.
[17] J. Gratton, C. Vigo, Self-similar gravity currents with variable inflow revisited: plane currents, J. Fluid Mech. 258 (1994) 77–104.
[18] A.J. Hogg, M. Ungarish, H.E. Huppert, Particle-driven gravity currents: asymptotic and box-model solutions, Eur. J. Mech. B Fluids 19 (2000) 139–165.
[19] A.C. Slim, H.E. Huppert, Self-similar solutions of the axisymmetric shallow-water equations governing converging inviscid gravity currents, J. Fluid Mech. 506 (2004) 331–355.
[20] R.T. Bonnecaze, M.A. Hallworth, H.E. Huppert, J.R. Lister, Axisymmetric particle-driven gravity currents, J. Fluid Mech. 294 (1995) 93–121.
[21] H.E. Huppert, The propagation of two-dimensional and axisymmetric viscous gravity currents over a rigid horizontal surface, J. Fluid Mech. 121 (1982) 43–58.
[22] R.T. Bonnecaze, H.E. Huppert, J.R. Lister, Particle-driven gravity currents, J. Fluid Mech. 250 (1993) 339–369.
[23] K.W. Morton, D.F. Mayers, Numerical Solutions of Partial Differential Equations, Cambridge University Press, 1994.
[24] W.H. Press, S.A. Teukolski, W.T. Vetterling, B.P. Flannery, Numerical Recipes in Fortran, Cambridge University Press, 1992.
[25] M. Ungarish, T. Zemach, On axisymmetric rotating gravity currents: two-layer shallow-water and numerical solutions, J. Fluid Mech. 481 (2003) 37–66.
[26] M. Ungarish, H.E. Huppert, On gravity currents propagating at the base of a stratified ambient: effects of geometrical constraints and rotation, J. Fluid Mech. 521 (2004) 69–104.
[27] R. Manasseh, C.-Y. Ching, H.J.S. Fernando, The transition from density-driven to wave-dominated isolated flows, J. Fluid Mech. 361 (1998) 253–274.